Table 1. Linearity of Doxorubicinone and Its Metabolites

	Slope			Intercept		r^2
	Mean	S.D.	Precision (%)	Mean	S.D.	
Doxorubicinol	12.71	0.22	1.73	0.0012	0.0062	1.000
Doxorubicin	12.16	0.19	1.56	−0.0009	0.0026	1.000
Doxorubicinolone	10.89	0.22	2.04	0.0029	0.0073	0.999
7-Deoxydoxorubicinolone	14.07	0.31	2.20	0.0049	0.0069	0.999

Precision (%): expressed as % R.S.D. (S.D./mean)×100.

Table 2. Detection Limit and Quantification Limit of Doxorubicin and Its Metabolites

	Doxorubicinol	Doxorubicine	Doxorubicinolone	7-Deoxydoxorubicinolone
Detection limit (pg)	3.8	4.9	6.4	7.4
Quantification limit (pg)	12.8	16.4	21.4	24.5

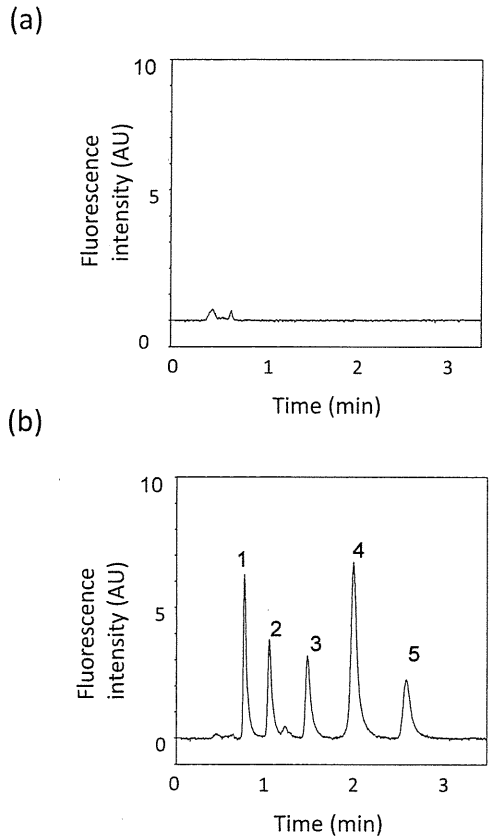

Fig. 2. Chromatograms of (a) Mouse Plasma and (b) Mouse Plasma Spiked with Doxorubicin and Its Metabolites

The chromatographic conditions are described in Experimental. AU; Arbitrary units. 1, doxorubicinol; 2, doxorubicin; 3, doxorubicinolone; 4, daunorubicin (internal standard); 5, 7-deoxydoxorubicinolone.

by isolating and identifying urinary metabolites, the metabolites retained doxorubicin's specific fluorescence properties.[15] Therefore, in this report, we used the fluorescent detection condition optimized for doxorubicin. Although the metabolites in human urine contained sulfate and glucuronide conjugates, which conjugate reactions also occur in liver, these conjugates were not detected in mouse plasma in our study. When a standard solution of doxorubicin, doxorubicinol, doxorubicinolone, 7-deoxydoxorubicinolone, and an internal standard (daunorubicin (Fig. 1b)) was analyzed, all compounds were separated within 3 min with good resolution (Fig. 2). The chromatogram of mouse plasma demonstrates the lack of chromatographic interference from endogenous plasma components (Fig. 2a). In a chromatogram of plasma spiked with doxorubicin and its metabolites at a concentration of 20 ng/mL, no interfering peaks were observed, and doxorubicin, the three metabolites, and the internal standard were well separated (Fig. 2b). These results show that the specificity of this method. We created calibration plots for doxorubicin and its metabolites. The plasma calibration curve was constructed using six calibration standards (2.5—100 ng/mL). The plots of relative peak area to IS *versus* concentration were linear over a wide range of concentrations (r^2=0.999—1.000) (Table 1). The detection limit and quantification limit were 3.8—7.4 pg and 12.8—24.5 pg injected compounds, respectively (signal to noise ratio, 3 : 1 for detection limits and 10 : 1 for quantitation limit). These values were 5 times lower than the limits ever reported using conventional HPLC[12,13,16—19] (Table 2).

We next tested the recovery of doxorubicin and its metabolites from mouse plasma spiked with each compound. The recovery rate was satisfactory, and the values for doxorubicinol, doxorubicin, doxorubicinolone, and 7-deoxydoxorubicinolone were 102.7, 92.6, 94.7, 96.7%, respectively (n=3). Tables 3 and 4 shows the accuracy and precision data for intra- and inter-day plasma samples. The assay values on both occasions (intra- and inter-day) were found to be within the accepted variable limits.[20]

The predicted concentrations for each analyte deviated within ±15% of the nominal concentrations in a series of stability test; in-injector (20 h), bench top (6 h), repeated three freeze/thaw cycles and at −80°C for at least 2 weeks (Table 5). Although 7-deoxydoxorubicinolone was slightly unstable under in-injector (20 h; 91.24%), other compounds were stable at any storage conditions.

We then used the validated method described above for the simultaneous detection of doxorubicin and its metabolites in mouse plasma after intravenous administration of doxorubicin. Doxorubicin and its metabolites doxorubicinol and 7-deoxydoxorubicinolone were detected in the plasma sample. Although doxorubicinolone has been also reported to be produced by NADP-dependent cytochrome P450 reductase,[13,15] it was not detected in this study (Fig. 3). Doxorubicinol is produced by cytosolic carbonyl reductase through the

Table 3. Intra-Day Assay Precision and Accuracy for Doxorubicin and Its Metabolites in Mouse Plasma

ng/mL	Doxorubicinol				Doxorubicin				Doxorubicinolone				7-Deoxydoxorubicinolone			
	Mean	S.D.	Precision	Accuracy	Mean	S.D.	Precision	Accuracy	Mean	S.D.	Precision	Accuracy	Mean	S.D.	Precision	Accuracy
5	5.12	0.41	8.08	102.45	4.98	0.15	3.03	99.56	4.82	0.61	12.73	96.30	4.70	0.44	9.42	93.90
25	25.16	1.40	5.55	100.63	25.46	0.88	3.47	101.84	23.56	1.39	5.92	94.24	25.75	1.25	4.84	102.99
100	99.78	0.94	0.94	99.78	99.55	0.99	1.00	99.55	99.49	1.21	1.22	99.49	99.47	1.13	1.14	99.47

Precision (%): expressed as % R.S.D. (S.D./mean)×100. Accuracy (%): calculated as (mean determined concentration/nominal concentration)×100.

Table 4. Inter-Day Assay Precision and Accuracy for Doxorubicin and Its Metabolites in Mouse Plasma

ng/mL	Doxorubicinol				Doxorubicin				Doxorubicinolone				7-Deoxydoxorubicinolone			
	Mean	S.D.	Precision	Accuracy	Mean	S.D.	Precision	Accuracy	Mean	S.D.	Precision	Accuracy	Mean	S.D.	Precision	Accuracy
5	5.13	0.16	3.04	102.51	5.35	0.49	9.18	107.05	5.31	0.35	6.55	106.18	4.95	0.11	2.25	98.95
25	24.31	0.68	2.81	97.24	23.74	0.38	1.59	94.96	24.84	0.42	1.69	99.34	24.56	0.37	1.52	98.24
100	99.83	0.48	0.48	99.83	100.11	1.13	1.13	100.11	100.39	0.32	0.32	100.39	99.83	0.44	0.44	99.83

Precision (%): expressed as % R.S.D. (S.D./mean)×100. Accuracy (%): calculated as (mean determined concentration/nominal concentration)×100.

Table 5. Stability Data in Mouse Plasma

	Doxorubicinol				Doxorubicin				Doxorubicinolone				7-Deoxydoxorubicinolone			
	Mean	S.D.	Precision	Accuracy	Mean	S.D.	Precision	Accuracy	Mean	S.D.	Precision	Accuracy	Mean	S.D.	Precision	Accuracy
5 ng/mL																
20 h (in-injector)	5.00	0.068	1.37	100.06	5.22	0.072	1.37	104.30	5.19	0.058	1.12	103.86	4.56	0.074	1.62	91.24
6 h (bench-top)	5.19	0.10	2.01	103.71	5.43	0.11	2.08	108.66	5.22	0.11	2.01	104.38	4.92	0.073	1.48	98.39
2 weeks at −80°C	4.72	0.12	2.43	94.36	5.23	0.14	2.62	104.54	5.21	0.082	1.58	104.20	4.98	0.092	1.84	99.59
3rd freeze-thaw	4.80	0.17	3.49	96.00	5.16	0.18	3.51	103.23	5.01	0.22	4.48	100.19	4.97	0.154	3.09	99.42
50 ng/mL																
20 h (in-injector)	51.27	1.48	2.89	102.53	54.10	2.07	3.82	108.20	47.08	1.54	3.28	94.16	50.69	1.77	3.49	101.38
6 h (bench-top)	53.78	2.90	5.39	107.55	52.12	2.76	5.30	104.25	49.66	2.27	4.56	99.32	54.33	2.36	4.33	108.66
2 weeks at −80°C	47.75	0.54	1.13	95.49	48.10	0.47	0.97	96.21	49.04	0.35	0.71	98.08	47.99	0.44	0.91	95.98
3rd freeze-thaw	52.09	0.81	1.56	104.18	51.04	0.81	1.59	102.08	48.68	0.95	1.96	97.37	51.52	0.86	1.68	103.04

Precision (%): expressed as % R.S.D. (S.D./mean)×100. Accuracy (%): calculated as (mean determined concentration/nominal concentration) ×100.

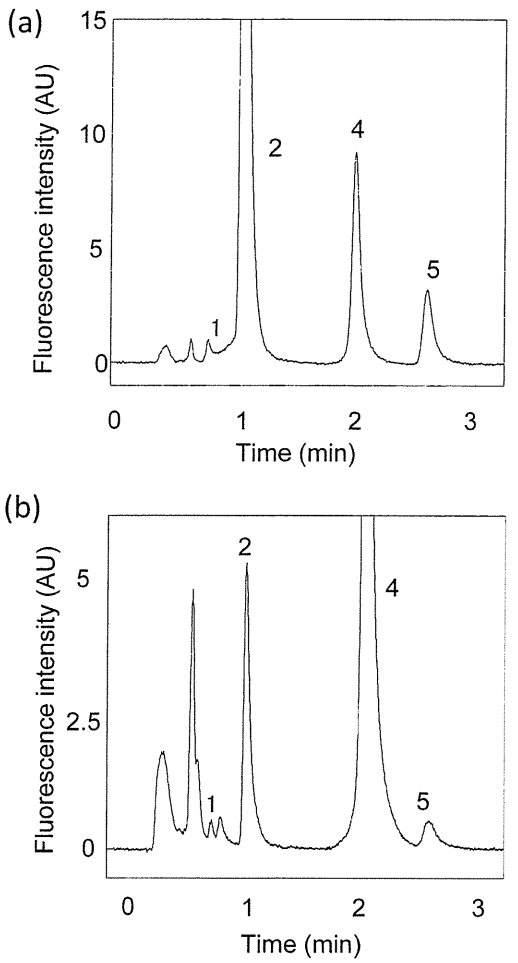

Fig. 3. Chromatogram of Mouse Plasma Obtained after Intravenous Administration of Doxorubicin

Doxorubicin (10 mg/kg) was administered by tail vein injection. Blood was removed from the tail vein after 10 min (a) and 6 h (b) of administration, and plasma was prepared as described in Experimental. 1, doxorubicinol; 2, doxorubicin; 4, daunorubicin (internal standard); 5,7-deoxydoxorubicinolone.

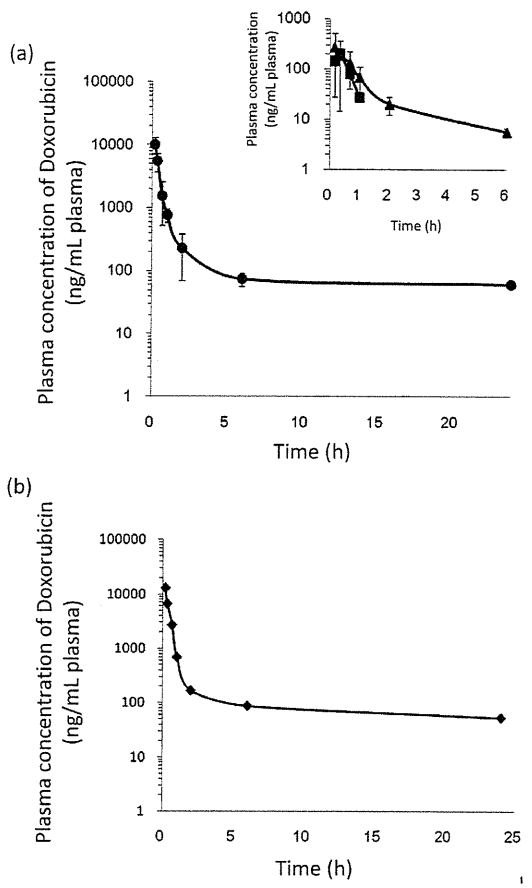

Fig. 4. Changes in Plasma Concentration over Time

Blood was collected from tail veins 10, 20, or 30 min or 1, 2, 6, or 24 h after administration of doxorubicin, and the drug concentrations in the plasma were measured. (Averaged results from 3 mice (a) and result of one mouse (b).) Main graph, doxorubicin. Inset, metabolites (squares: doxorubicinol; triangles: 7-deoxydoxorubicinolone).

NADPH-dependent aldo-keto reduction of a carbonyl moiety in doxorubicin[15]; deglycosidation at the daunosamine sugar in doxorubicin or doxorubicinol produces 7-deoxydoxorubicinolone[15,21] (Fig. 1a). The major metabolites we detected were coincident with those reported previously.[22] We also examined the time course of changes in the concentrations of doxorubicin and its metabolites (Fig. 4a). After an initial rapid decrease, the doxorubicin concentration decreased slowly, and the plasma concentration of doxorubicin was 74.2 ng/mL (6 h) and 61.1 ng/mL (24 h) (n=3). The persistence of doxorubicin indicates that doxorubicin comes back very slowly from some distributed tissues or circulates for a relatively long time by binding to plasma proteins.[15]

The area under the curve (AUC_{0-24h}) and C_{max} of doxorubicin was 5.9 μg h/mL and 10.0 μg/mL, respectively, similar to the value of 4.16 μg h/mL, and 5.4 μg/mL obtained previously using a conventional HPLC method.[7] In addition, our method enabled us to trace the change in doxorubicin concentration over time in a single mouse (Fig. 4b); this had previously been difficult to do because of the small sample volumes. This property will allow us to minimize the number of animals needed for pharmacokinetic analyses. Furthermore, in a clinical setting, the small blood sample volumes and fast analytical time would reduce the impact of TDM on patients.

Conclusions

Our results show that the method we developed using UHPLC provides rapid analysis using very small plasma samples. The method is sensitive enough to evaluate changes in the concentrations of doxorubicin and its metabolites in a single mouse; this will result in the use of smaller numbers of animals, which is good for animal protection. In clinical applications, this method could also decrease the burden of TDM for patients. We predict that it will greatly facilitate studies of doxorubicin pharmacokinetics and clarify the effect of doxorubicin metabolism on therapeutic outcome.

Acknowledgements The authors are grateful for financial support from the Research on Publicly Essential Drugs and Medical Devices Project (The Japan Health Sciences Foundation); a Health Labor Sciences Research Grant from the Ministry of Health, Labour, and Welfare (MHLW); and KAKENHI (21790046) from the Ministry of Education, Culture, Sports, Science and Technology (MEXT) of Japan.

References

1) Hortobágyi G. N., *Drugs*, **54** (Suppl. 4), 1—7 (1997).
2) Di Marco A., Gaetani M., Scarpinato B., *Cancer Chemother. Rep.*, **53**, 33—37 (1969).
3) O'Brien M. E., Wigler N., Inbar M., Rosso R., Grischke E., Santoro A., Catane R., Kieback D. G., Tomczak P., Ackland S. P., Orlandi F., Mellars L., Alland L., Tendler C., CAELYX Breast Cancer Study Group, *Ann. Oncol.*, **15**, 440—449 (2004).
4) Olson R. D., Mushlin P. S., Brenner D. E., Fleischer S., Cusack B. J., Chang B. K., Boucek R. J. Jr., *Proc. Natl. Acad. Sci. U.S.A.*, **85**, 3585—3589 (1988).
5) van Asperen J., van Tellingen O., Beijnen J. H., *Drug Metab. Dispos.*, **28**, 264—267 (2000).
6) Yokoyama M., Okano T., Sakurai Y., Fukushima S., Okamoto K., Kataoka K., *J. Drug Target.*, **7**, 171—186 (1999).
7) Nakanishi T., Fukushima S., Okamoto K., Suzuki M., Matsumura Y., Yokoyama M., Okano T., Sakurai Y., Kataoka K., *J. Controlled Release*, **74**, 295—302 (2001).
8) Sakai-Kato K., Saito E., Ishikura K., Kawanishi T., *J. Chromatogr. B Analyt. Technol. Biomed. Life Sci.*, **878**, 1466—1470 (2010).
9) Swartz M. E., *J. Liq. Chrom. Rel. Technol.*, **28**, 1253—1263 (2005).
10) Nováková L., Vlcková H., *Anal. Chim. Acta*, **656**, 8—35 (2009).
11) Sun N., Lu G., Lin M., Fan G., Wu Y., *Talanta*, **78**, 506—512 (2009).
12) van Asperen J., van Tellingen O., Beijnen J. H., *J. Chromatogr. B Biomed. Sci. Appl.*, **712**, 129—143 (1998).
13) Zhou Q., Chowbay B., *J. Pharm. Biomed. Anal.*, **30**, 1063—1074 (2002).
14) Maudens K. E., Stove C. P., Lambert W. E., *J. Sep. Sci.*, **31**, 1042—1049 (2008).
15) Takanashi S., Bachur N. R., *Drug Metab. Dispos.*, **4**, 79—87 (1976).
16) Andersen A., Warren D. J., Slørdal L., *Ther. Drug Monit.*, **15**, 455—461 (1993).
17) Shinozawa S., Mimaki Y., Araki Y., Oda T., *J. Chromatogr.*, **196**, 463—469 (1980).
18) Rose L. M., Tillery K. F., el Dareer S. M., Hill D. L., *J. Chromatogr.*, **425**, 419—423 (1988).
19) Andersen A., Holte H., Slørdal L., *Cancer Chemother. Pharmacol.*, **44**, 422—426 (1999).
20) Guidance for Industry: Bioanalytical Method Validation. U.S. Department of Health and Human Services Food and Drug Administration (2001)
21) Lown J. W., *Pharmacol. Ther.*, **60**, 185—214 (1993).
22) van Asperen J., van Tellingen O., Tijssen F., Schinkel A. H., Beijnen J. H., *Br. J. Cancer*, **79**, 108—113 (1999).

International Journal of Pharmaceutics 423 (2012) 401–409

Contents lists available at SciVerse ScienceDirect

International Journal of Pharmaceutics

journal homepage: www.elsevier.com/locate/ijpharm

Pharmaceutical nanotechnology

Evaluation of intracellular trafficking and clearance from HeLa cells of doxorubicin-bound block copolymers

Kumiko Sakai-Kato[a,*], Keiko Ishikura[a], Yuki Oshima[a], Minoru Tada[b], Takuo Suzuki[b], Akiko Ishii-Watabe[b], Teruhide Yamaguchi[c], Nobuhiro Nishiyama[d], Kazunori Kataoka[d,e], Toru Kawanishi[c], Haruhiro Okuda[a]

[a] Division of Drugs, National Institute of Health Sciences, 1-18-1 Kamiyoga, Setagaya-ku, Tokyo 158-8501, Japan
[b] Division of Biological Chemistry and Biologicals, National Institute of Health Sciences, 1-18-1 Kamiyoga, Setagaya-ku, Tokyo 158-8501, Japan
[c] National Institute of Health Sciences, 1-18-1 Kamiyoga, Setagaya-ku, Tokyo 158-8501, Japan
[d] Center for Disease Biology and Integrative Medicine, Graduate School of Medicine, The University of Tokyo, 7-3-1 Hongo, Bunkyo-ku, Tokyo 113-0033, Japan
[e] Department of Materials Engineering, Graduate School of Engineering, The University of Tokyo, 7-3-1 Hongo, Bunkyo-ku, Tokyo 113-8656, Japan

ARTICLE INFO

Article history:
Received 1 July 2011
Received in revised form
16 November 2011
Accepted 15 December 2011
Available online 23 December 2011

Keywords:
Doxorubicin-bound block copolymers
Intracellular trafficking
Confocal microscopy
Transporter
Endocytosis

ABSTRACT

New technologies are needed to deliver medicines safely and effectively. Polymeric nanoparticulate carriers are one such technology under investigation. We examined the intracellular trafficking of doxorubicin-bound block copolymers quantitatively and by imaging doxorubicin-derived fluorescence using confocal microscopy. The polymers were internalized by endocytosis and distributed in endosomal/lysosomal compartments and the endoplasmic reticulum; unlike free doxorubicin, the polymers were not found in the nucleus. Moreover, the ATP-binding cassette protein B1 (ABCB1) transporter may be involved in the efflux of the polymer from cells. This drug delivery system is attractive because the endogenous transport system is used for the uptake and delivery of the artificial drug carrier to the target as well as for its efflux from cells to medium. Our results show that a drug delivery system strategy targeting this endogenous transport pathway may be useful for affecting specific molecular targets.

1. Introduction

Recently, genomic drug discovery techniques, organic synthesis, and screening technologies have been used to develop molecularly targeted medicines, some of which are already being used clinically (Hopkins and Groom, 2002; Hughes, 2009). However, these new technologies do not necessarily lead to the introduction of new treatments because even when promising compounds are discovered by genomic drug discovery techniques, they often have harmful properties or are difficult to deliver to the target because they are relatively insoluble (Hopkins and Groom, 2002; Lipinski et al., 2001). New formulation technologies are being developed to enhance the effectiveness and safety of pharmaceutical products by focusing on improving the release, targeting, and stability of drugs within the body, so that the location and timing of their action in the living body can be controlled.

Nanotechnological advances have contributed to the development of new drug delivery system (DDS) products such as polymeric micelles and liposomes that range in size from several tens of nanometers to 100 nm (Ferrari, 2005). Some of these DDS products are already being marketed as innovative medical treatments (O'Brien et al., 2004), and the number being used in clinical trials has risen impressively in recent years (Hamaguchi et al., 2007; Kuroda et al., 2009; Matsumura et al., 2004). These nanoparticulates possess several unique advantages for drug delivery, including high drug-loading capacity, controlled drug release, and small size, which allows the drug to accumulate in pathological tissues such as tumors, which have increased vascular permeability (Nishiyama and Kataoka, 2006).

Polymeric micelles have received considerable attention recently as promising macromolecular carrier systems (Allen et al., 1999; Kataoka et al., 1993, 2001; Lavasanifar et al., 2002; Torchilin, 2002; Torchilin et al., 2003). Polymeric micelles are amphipathic systems in which a hydrophobic core is covered with an outer

Abbreviations: DDS, drug delivery system; PEG, polyethyleneglycol; RES, reticuloenodothelial system; EPR, enhanced permeability and retention; Dox, doxorubicin; DMEM, Dulbecco's modified Eagle's medium; FBS, fetal bovine serum; DLS, dynamic light scattering; AFM, atomic force microscopy; HBSS, Hank's balanced salt solution; ER, endoplasmic reticulum; ECFP, enhanced cyan fluorescent protein; Alexa-transferrin, Alexa Fluor 488 conjugate of transferrin; MTOC, microtubule-organizing center; ABCB1, ATP-binding cassette protein B1; MDR1, multidrug resistance 1; (PBS), phosphate-buffered saline; EDTA, ethylenediamine tetraacetic acid; SDS, sodium dodecyl sulfate; PVDF, polyvinylidene fluoride.

* Corresponding author. Tel.: +81 3 3700 9662; fax: +81 3 3700 9662.
E-mail address: kumikato@nihs.go.jp (K. Sakai-Kato).

0378-5173/$ – see front matter © 2011 Elsevier B.V. All rights reserved.
doi:10.1016/j.ijpharm.2011.12.022

shell consisting of hydrophilic macromolecules such as polyethylene glycol (PEG) chains. Polymeric micelles can both encapsulate medicine of high density and evade the foreign body recognition mechanism within the reticuloendothelial system (RES), and they show excellent retention in the blood (Illum et al., 1987). In addition, accurate size control of the nanoparticulates enables them to accumulate in cancerous tissue, owing to the increased permeability of tumor vessels due to the enhanced permeability and retention (EPR) effect (Matsumura and Maeda, 1986).

To maximize the efficacy and safety of DDS products, it is important to deliver these products to specific target cells and subcellular compartments. In the experiments reported here, we used confocal microscopy to study the intracellular trafficking of polymeric nanoparticulate carriers. The use of covalently bound fluorescent reagents as probes is gradually clarifying the internalization pathways and intracellular localizations of polymeric nanoparticulate carriers (Lee and Kim, 2005; Manunta et al., 2007; Murakami et al., 2011; Rejman et al., 2005; Richardson et al., 2008; Sahay et al., 2008; Savić et al., 2003). However, the excretion of the polymers from target cells after they have released the incorporated drugs has not yet been clarified in detail, although information about the clearance of carriers from cells is important from the perspective of safety. In this study, we examined the trafficking of a polymeric nanoparticulate carrier in detail, including the efflux of the polymers from cells to medium, by direct measurement of doxorubicin (Dox) covalently bound to the block copolymer. This technique avoids the necessity of considering the effects of exogenously tagged fluorescent probes on the intracellular trafficking.

Dox is one of the most effective available anticancer drugs in spite of its severe toxic effects, especially cardiotoxicity (Olson et al., 1988). As the carrier we used a PEG-poly(aspartic acid) block copolymer with covalently bound Dox (Fig. 1) (Yokoyama et al., 1999), because Dox has relevant hydrophobicity to form globular micelles by means of the hydrophobic interactions, and inherent fluorescence to investigate the intracellular trafficking of the carrier itself. Dox is partially covalently bound to the side chain of the aspartic acid (about 45% of aspartic acids), so that prepared Dox-conjugated block copolymers show good Dox entrapment efficiency possibly due to the π–π interaction between conjugated and incorporated Dox molecules (Bae and Kataoka, 2009; Nakanishi et al., 2001). Therefore, in this carrier system, there are two kinds of Dox; one is Dox covalently bound to block copolymers, and the other is free Dox which is incorporated in the inner core and has a pharmacological activity by its release from the inner core. The inner core of the micelles is greatly hydrophobic owing to the conjugated Dox, while the PEG of the outer layer prevents uptake by the RES. The resulting micelle effectively accumulates in tumor tissue by the EPR effect and shows much stronger activity than free Dox (Nakanishi et al., 2001). Because the block copolymer can form globular micelles by means of hydrophobic interactions with the conjugated Dox, as shown in Section 3.1, we used a carrier without incorporated free Dox to investigate the intracellular trafficking of the carrier itself. Furthermore, by quantifying directly the amount of Dox covalently bound to the polymers, we could measure the intracellular amount of the polymers.

2. Materials and methods

2.1. Cells and micelles

HeLa cells (Health Science Research Resources Bank, Osaka, Japan) were kept in Dulbecco's modified Eagle's medium (DMEM; Invitrogen Corp., Carlsbad, CA, USA) supplemented with 10% fetal bovine serum (FBS; Nichirei Biosciences Inc., Tokyo, Japan) and 100 U/mL penicillin/streptomycin (Invitrogen). Cells were grown in a humidified incubator at 37 °C under 5% CO_2. Dox-bound polymeric micelles and fluorescent dye (DBD)-labeled PEG-polyaspartate block copolymers partially modified with 4-phenyl-1-butanol were synthesized by Nippon Kayaku Co. Ltd. (Tokyo, Japan) (Nakanishi et al., 2001).

2.2. Physicochemical data of Dox-bound micelles

The diameters and distribution of micelles were determined by using dynamic light scattering (DLS; Zetasizer Nano ZS, Malvern, UK) at 25 °C. The micelles were dissolved in water and filtered through a 0.2-μm filter before measurement. Atomic force microscopy (AFM) measurements were conducted with a NanoWizard II (JPK Instruments, Berlin, Germany) at room temperature. Images were obtained in tapping mode using a commercial microcantilever with a spring constant of 150 N/m (Olympus Corporation, Tokyo, Japan). AFM images were processed with SPM image processing v. 3 software from JPK Instruments.

2.3. Quantitation of Dox-bound polymers in HeLa cells

The amounts of Dox-bound polymers in HeLa cells were determined by measuring the amount of doxorubicinone, which is released by acid hydrolysis of Dox-bound polymers (Fig. 1b). HeLa cells (1.5×10^5) were plated in 35-mm glass-bottom dishes coated with poly-L-lysine (Matsunami, Osaka, Japan) in DMEM containing 10% FBS and 100 U/mL penicillin/streptomycin. After incubation for two days (37 °C, 5% CO_2), the cells were exposed to 50 μg/mL Dox-bound polymers in culture medium. After the indicated durations, the cells were washed and kept in phosphate-buffered saline (PBS) or Hank's balanced salt solution (HBSS; Invitrogen). The cells were trypsinized with 0.25% trypsin-ethylenediamine tetraacetic acid (EDTA) (Invitrogen) and collected. Cells were then washed with PBS three times, and a small part of the cell suspension was used for cell counting. After centrifugation at 1000 rpm for 5 min, cell pellets were resuspended in 100 μL PBS, and the suspension was divided into two parts (50 μL was used with acid hydrolysis and 50 μL without) and stored at −80 °C until analysis. After thawing, the cell suspensions were disrupted by ultrasonic liquid processor (ASTRASON 3000, Misonix, NY, USA) for 1 min. Then, 50 μL of suspension was hydrolyzed by 0.5 N HCl at 50 °C for 15 h. After hydrolysis, samples were deproteinized with methanol, followed by centrifugation at 15,000 × *g* for 5 min at 4 °C. The supernatant was then neutralized with ammonium buffer, and evaporated to dryness under reduced pressure (Savant SpeedVac concentrator, Thermo Fisher Scientific, MA, USA). The residues were resuspended in 60% methanol, and the doxorubicinone released from the polymers by acid hydrolysis was quantified by ultra-high-performance liquid chromatography by using our previously reported method (Sakai-Kato et al., 2010) to determine the amount of intracellular Dox-bound polymers (Fig. 1b). The other 50 μL of cell suspension was treated in the same way but without the hydrolysis step to evaluate the amount of free doxorubicinone, that is, doxorubicinone not derived from Dox-bound polymers. The results of three independent experiments were averaged and analyzed statistically by *t*-test.

2.4. In vitro cytotoxicity

HeLa cell lines were evaluated in the present study. The HeLa cells were maintained in monolayer cultures in DMEM containing 10% FBS and 100 U/mL penicillin/streptomycin. WST-8 Cell Counting kit-8 (Dojindo, Kumamoto, Japan) was used for cell proliferation assay. 3000 cells of HeLa cell line in 100 μL of culture medium were plated in 96 well plates and were then incubated for 24 h at 37 °C. Serial dilutions of Dox-bound polymers, micelles incorporating free Dox or just free Dox were added, and the cells were incubated for 24

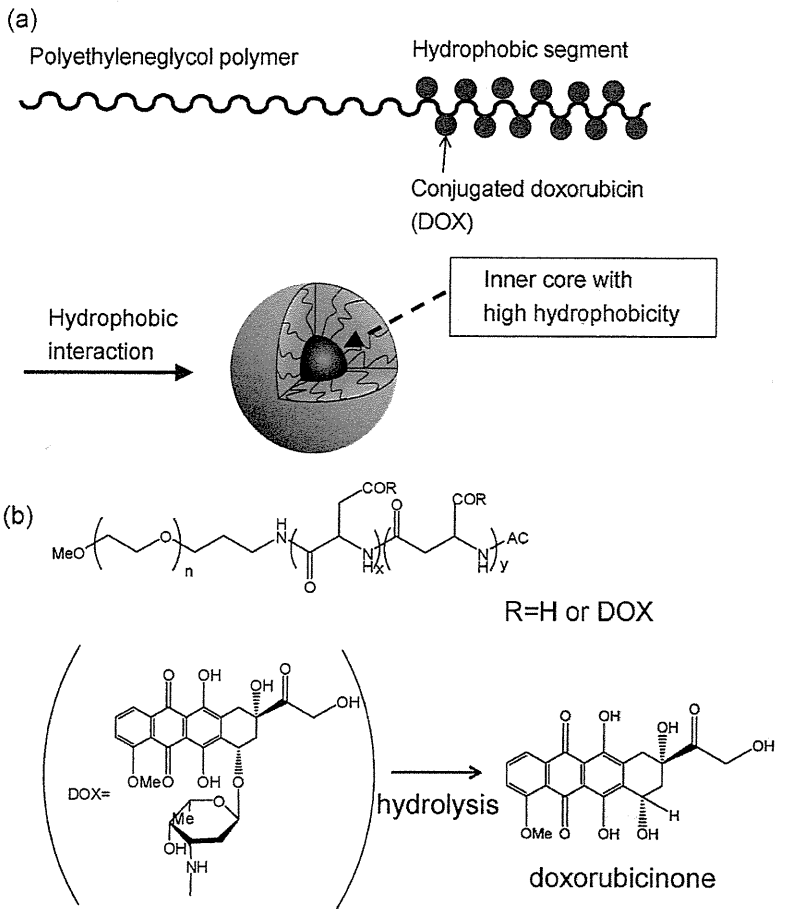

Fig. 1. Schematic of the structure of a Dox-bound polymeric micelle (a) and the chemical structure of the block copolymer (b). Polymer-bound Dox can be released as doxorubicinone by acid hydrolysis. The quantity of released doxorubicinone was used as a measure of the amount of intracellular polymers.

or 48 h. All data were expressed as mean ± SD of triplicate data. The data were then plotted as a percentage of the data from the control cultures, which were treated identically to the experimental cultures, except that no drug was added.

2.5. Confocal analysis of live cells

The intracellular trafficking of the Dox-bound micelles in live cells was examined by confocal microscopy (Carl Zeiss LSM 510, Oberkochen, Germany, or Nikon A1, Tokyo, Japan). Data were collected using dedicated software supplied by the manufacturers and exported as tagged image files (TIFs). HeLa cells (1.5×10^5) were plated in 35-mm glass-bottom dishes coated with poly-L-lysine (Matsunami) in DMEM containing 10% FBS and 100 U/mL penicillin/streptomycin. After incubation for two days (37 °C, 5% CO_2), the cells were exposed to 50 μg/mL Dox-bound polymers in culture medium. After the indicated durations, the cells were washed and kept in PBS or HBSS (Invitrogen) for imaging with the confocal microscope.

2.6. Labeling specific organelles in live cells

After incubation with Dox-bound polymers for 24 h, HeLa cells were washed with HBSS and labeled with organelle-specific fluorescent probes in accordance with the manufacturer's instructions. LysoTracker probe (Invitrogen) was used for labeling lysosomes, and ER-Tracker (Invitrogen) was used for labeling the endoplasmic reticulum (ER). A fluorescent Alexa Fluor 488 conjugate of transferrin (Alexa-transferrin; Invitrogen) was used as an exogenously added endocytic marker to delineate the endocytic recycling pathway for live cell imaging.

We also used an expression construct containing enhanced cyan fluorescent protein (ECFP) fused to an Golgi-targeting sequence derived from human β-1,4-galactosyltransferase as an Golgi localization marker (ECFP-Golgi). The construct was purchased from Clontech (Takara Bio Inc., Shiga, Japan). Cells were grown in 35-mm glass-bottom dishes coated with poly-L-lysine and transfected with Lipofectamine 2000 (Invitrogen). After overnight incubation, the cells were exposed to and allowed to internalize Dox-bound micelles for 24 h and then examined with confocal microscopy.

2.7. Efflux study of DOX-bound polymers or DBD-labeled polymers using the ABCB1 inhibitor verapamil

HeLa cells (1.5×10^5) were plated in 35-mm glass-bottom dishes coated with poly-L-lysine in DMEM containing 10% FBS and 100 U/mL penicillin/streptomycin. After incubation for two days (37 °C, 5% CO_2), the cells were exposed to 50 μg/mL Dox-bound polymers in culture medium for 3 h. Cells were washed with 50 μg/mL verapamil (Wako Pure Chemical Industries, Ltd., Osaka, Japan) (Davis et al., 2004; Kolwankar et al., 2005) or 0.1% dimethyl sulfoxide as a control. After washes, the cells were incubated for another 2 h in HBSS containing the same concentration of reagent. The cells were collected and processed for measurement of intracellular concentrations of Dox-bound polymers as described in Section 2.3. The efflux of DBD-labeled polymers was evaluated by

measurement of the fluorescent intensity inside cells using confocal microscopy. The intensity of the intracellular fluorescence was evaluated by image processing software (MetaMorph, Molecular Devices, CA, USA). The intensity of a single cell was mathematically determined by dividing the total intensity by the number of cells. Three independent experiments were averaged and analyzed statistically with the *t*-test.

2.8. Knockdown of ABCB1 by siRNA

Stealth RNAi oligonucleotides (Invitrogen) were used for siRNA experiments. Human ABCB1-siRNA sense, 5′-UCCCGUAGAAACCUUACAUUUAUGG-3′, and antisense, 5′-CCAUAAAUGUAAGGUUUCUACGGGA-3′, sequences were used. For a negative control, the Stealth RNAi Low GC Negative Control Duplex (Invitrogen) was used. The Stealth RNAi oligonucleotides were transfected into HeLa cells by using Lipofectamine RNAi MAX according to the manufacturer's protocols. After two days, the cells were exposed to 50 μg/mL Dox-bound polymers in culture medium for 3 h. After incubation, cells were washed with HBSS, and then incubated for another 2 h in HBSS without polymers. Cells were collected, and the intracellular polymers were quantified as described in Section 2.3.

2.9. Western blotting

Cells were washed with PBS and lysed in lysis buffer (20 mM Tris-HCl, pH 7.5; 1 mM EDTA; 10% glycerol; and 1% Triton X-100) containing protease inhibitors, namely, 2 mM phenylmethylsulfonyl fluoride and protease inhibitor cocktail (Sigma-Aldrich, St. Louis, MO, USA). Samples were electrophoresed on a sodium dodecyl sulfate (SDS)-polyacrylamide gel (5–20%) and transferred to a Polyvinylidene fluoride (PVDF) membrane. The blots were probed with anti-MDR (G-1) antibody (Santa Cruz Biotechnology, Inc., Santa Cruz, CA, USA) and developed with anti-mouse IgG peroxidase-linked species-specific whole antibody (from sheep) (GE Healthcare UK Limited, Little Chalfont, UK) by chemiluminescence.

3. Results and discussion

3.1. Physicochemical properties of Dox-bound micelles

The micelle carrier (Fig. 1) consisted of a block copolymer of PEG (molecular weight about 5000) and poly(aspartic acid) (polymerization degree, 30). To increase the hydrophobicity of the inner core, Dox was partially conjugated (about 45%) to the side chain of the aspartic acid. Because particle size affects the intracellular uptake of nanoparticulate formulations, we first examined the particle size of the micelles without free Dox. The Dox-bound micelles had a hydrodynamic diameter of about 42 nm at the dosed concentration of 50 μg/mL (Fig. 2a). AFM measurement of the micelles also confirmed that they were spherical with a particle size of around 40 nm (Fig. 2b). This size of micelle without free Dox is very similar to that of the micelles containing free Dox in the inner core that interacts with the conjugated Dox (Nakanishi et al., 2001), indicating that the presence of incorporated free Dox does not change the average diameter much.

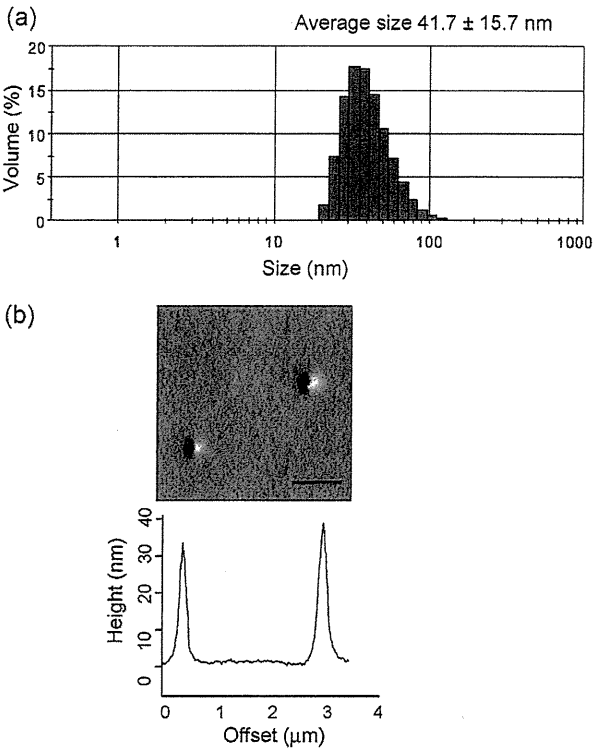

Fig. 2. Physicochemical properties of Dox-bound polymeric micelles. (a) Average size distribution of Dox-bound polymeric micelles by DLS. (b) The upper image shows an AFM image of Dox-bound polymeric micelles (bar: 1 μm) and the lower shows the cross-sectional topological profile of the image drawn in the upper panel.

3.2. In vitro cytotoxicity

We examined the *in vitro* cytotoxicity of the Dox-bound copolymers and the micelles incorporating free doxorubicin. As shown in Table 1, the cytotoxicity of doxorubicin-bound copolymers was negligible. This fact has been also reported in the previously published paper (Nakanishi et al., 2001). On the other hand, micelles incorporating free doxorubicin showed equivalent *in vitro* cytotoxic activity to free doxorubicin which is not incorporated into micelle. Therefore, in this system, the doxorubicin was conjugated to the block copolymer to increase the hydrophobicity of the inner core of the micelle so that efficient amount of free doxorubicin can be incorporated into the inner core of the micelles, and its cytotoxicity was negligible.

3.3. Intracellular uptake of Dox-bound polymers

To evaluate the intracellular uptake of Dox-bound polymers, we measured their intracellular amount by quantitating the doxorubicinone released from the intracellular polymers by acid hydrolysis treatment (Fig. 1b). Although the Dox-bound polymers contained 0.02% (w/w) free doxorubicinone as an impurity, no inherent free doxorubicinone was detected in the cells in any of the experiments in which we measured the intracellular concentration of doxorubicinone without acid hydrolysis. This result also indicates that

Table 1
IC50 values (μg/mL).

24 h			48 h		
Dox-bound polymer	Micelle incorporating free Dox	Free Dox	Dox-bound polymer	Micelle incorporating free Dox	Free Dox
>10	0.37	0.27	>10	0.045	0.024

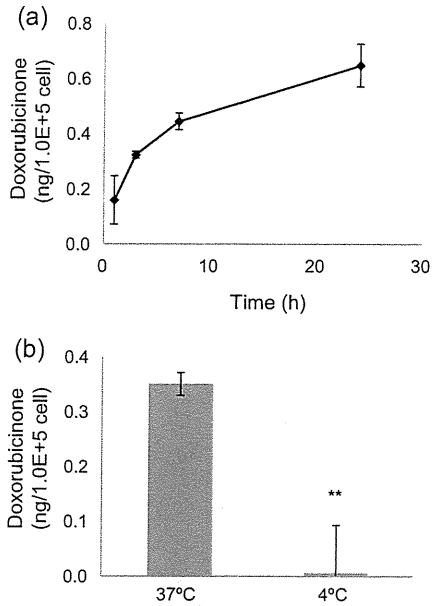

Fig. 3. Internalization of Dox-bound polymers. (a) Change in the internalized amount of Dox-bound polymers in cells as indicated by released doxorubicinone over time. HeLa cells were incubated in medium containing Dox-bound polymers for the indicated durations, followed by washes with PBS. The doxorubicinone released by acid hydrolysis was quantitated as a measure of the amount of intracellular polymers, as described in Section 2. (b) Effect of temperature on the internalization of Dox-bound polymers. HeLa cells were incubated in medium containing Dox-bound polymers at 37 °C or 4 °C for 3 h, followed by washes with PBS. The amount of intracellular polymers was quantitated by measuring the doxorubicinone released by acid hydrolysis, as described in Section 2. $^{**}P < 0.01$.

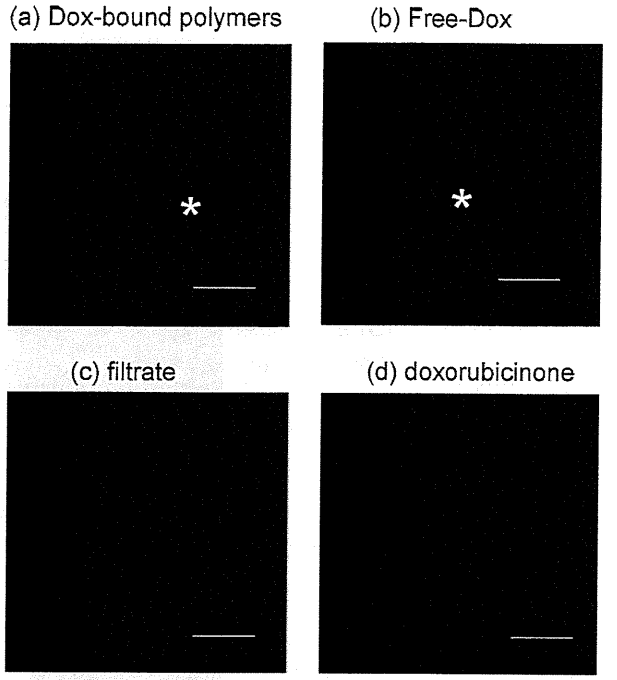

Fig. 4. Intracellular distribution of (a) DOX-bound polymers in HeLa cells exposed to 50 μg/mL Dox-bound polymers and (b) free DOX in cells exposed to 5 μg/mL free Dox for 1 h. Intracellular distribution of DOX-bound polymers in HeLa cells (c) cultured for 24 h in medium containing the filtrate of medium that was preincubated with Dox-bound polymers, and (d) cultured with 20 ng/mL free doxorubicinone for 24 h. Bars: 10 μm. Asterisk indicates the nucleus.

degradation of Dox-bound polymers that releases doxorubicinone during the experiments was negligible.

We then incubated HeLa cells in medium containing Dox-bound polymers for 1–24 h. After the incubation, the cells were washed. By determining the amounts of doxorubicinone released from Dox-bound polymers by acid hydrolysis of the cells, we were able to observe a time-dependent increase in the intracellular amount of Dox-bound polymers (Fig. 3a). Moreover, the amount of polymers in cells was significantly lower in cells incubated with the polymers at 4 °C than at 37 °C (Fig. 3b), indicating that the cells took up the polymers by endocytosis.

3.4. Intracellular distribution of Dox-bound polymers

The intracellular distribution of Dox-bound polymers was studied by confocal microscopy using the inherent fluorescence of the Dox covalently bound to the block copolymers. The Dox-bound polymers were localized in the perinuclear regions but not in the nucleus (Fig. 4a). This was different from the localization of free Dox which was distributed in the nucleus after 1 h (Fig. 4b), as reported previously (Beyer et al., 2001). This distribution will explain the fact that *in vitro* cytotoxicity of Dox-bound polymers was negligible (Table 1). To confirm that the Dox was not released from block copolymers as doxorubicinone (Fig. 1b) during the incubation time of the experiment, Dox-bound polymers were incubated in cell culture medium for 1 h at 37 °C, and then removed by centrifugal filtration using a Microcon YM-3 tube (Millipore, MA, USA). The resultant filtrate was added to the cell culture medium. Confocal microscopy showed no fluorescence within the cells (Fig. 4c). Furthermore, when HeLa cells were cultured in cell culture medium containing 20 ng/mL free doxorubicinone, which corresponds to 0.02% (w/w) of Dox-bound polymers, for 24 h, fluorescence was negligible within the cells (Fig. 4d). These results show that the fluorescence seen within the cells after Dox-bound polymer incubation is caused by the uptake of polymers and not by free doxorubicinone or Dox.

We next examined the intracellular localization of Dox-bound polymers by colocalization studies using fluorescent organelle markers. The fluorescence derived from Dox-bound polymers coincided well with the specific staining of the ER by ER-Tracker in double-labeling experiments (Fig. 5a). High-resolution images showed that both staining procedures clearly stained membranal structures (Fig. 5b).

Because the Golgi apparatus is also located in the perinuclear area and is involved in the intracellular transport of various molecules, we investigated the localization of the polymers by transfecting cells with an expression construct containing ECFP fused to a Golgi-specific protein. As shown in Fig. 5c, the distribution of polymers in the Golgi was negligible. We also confirmed that treatment of cells with Lipofectamine treatment did not affect the distribution of polymers (data not shown).

To what, then, can this particularly strong staining of the perinuclear areas be attributed? The perinuclear area is known to be the microtubule-organizing center (MTOC), an area in eukaryotic cells from which microtubules emerge and where endosomes and other endocytotic vesicles cluster (Matteoni and Kreis, 1987). In fact, a fluorescent staining image showed that the vesicles containing Dox-bound polymers in the perinuclear area (Fig. 6a, yellow arrows) coincided with the MTOC, as marked by Alexa-transferrin, an endocytic marker (Fig. 6a, white arrows). Some of the vesicles containing polymers were also stained by LysoTracker, a dye that specifically stains lysosomes (Fig. 6b). These results show that the polymers are internalized by endocytosis and transported to endosomal/lysosomal compartments. Duncan and colleagues, examined the localization of polymers by using Oregon Green as a fluorescent tag and found that three water-soluble polymeric carriers, *N*-(2-hydroxypropyl)methacrylamide, Dextran, and PEG, localized to late

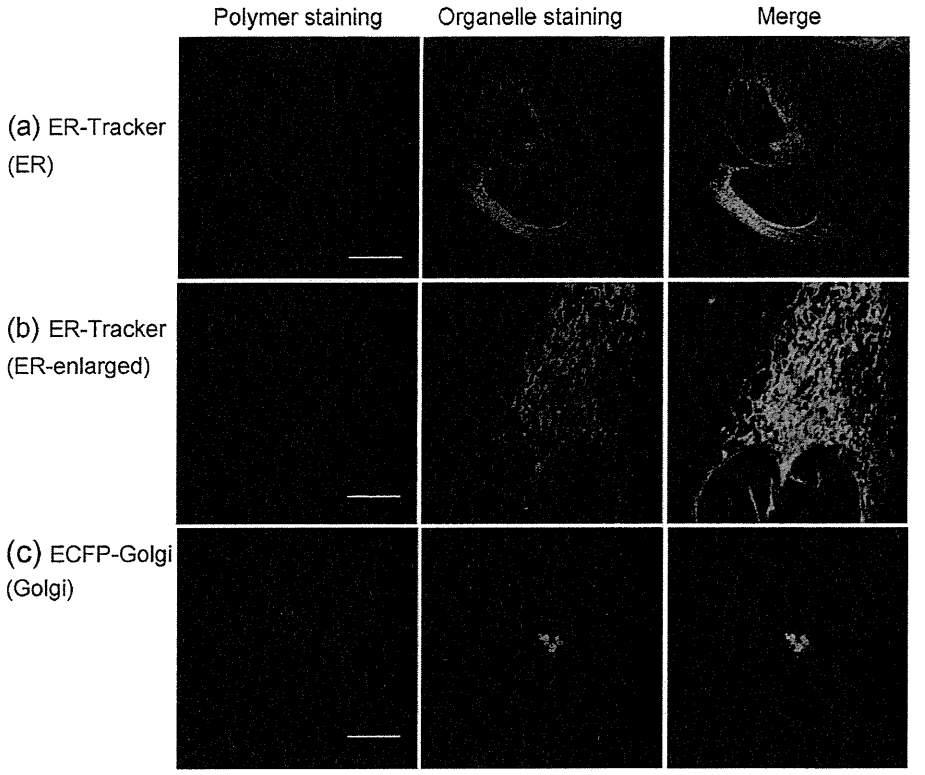

Fig. 5. Localization of Dox-bound polymers in cells co-stained with organelle-specific markers. Left, images of stained Dox-bound polymers; middle, organelle-specific fluorescent staining images; right, merged images of the left and middle images. Localization experiments using. (a and b) ER-Tracker for ER, (c) ECFP-Golgi for Golgi. Bars: 10 μm for (a) and (c). Bars: 5 μm for (b).

endosomal compartments (including lysosomes) (Richardson et al., 2008), findings consistent with our results. The perinuclear localization of the polymers is a great advantage of this system with regard to the incorporation of a nuclear-targeted drug or gene.

Most nanomaterials have been shown to exploit more than one pathway to gain cellular entry, and the pathway exploited can determine the intracellular fate (Sahay et al., 2010a). After internalization into HeLa cells, the Dox-bound polymers might be delivered to the ER directly from endosomes; in the case of cholesterol, there is some evidence for a direct pathway from endosomes to the ER (Ioannou, 2001; Mineo and Anderson, 2001). Or the polymers might be delivered to the ER directly, bypassing the endosomes/lysosomes, as do unimers of the amphiphilic triblock copolymer of poly(ethylene oxide), poly(propylene oxide), and Pluronic P85 (Sahay et al., 2010b). Simian virus 40 is known to enter the cytosol *via* the ER, suggesting that polymers distributed

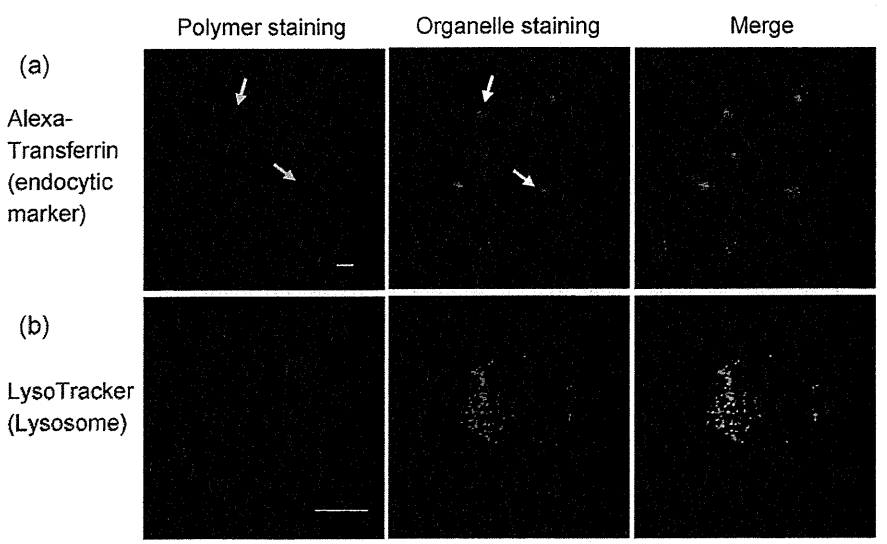

Fig. 6. Fluorescent staining images of Dox-bound polymers in cells co-stained with organelle-specific markers. Left, images of stained Dox-bound polymers; middle, organelle-specific fluorescent staining images; right, merged images of the left and middle images. Localization experiments using. (a) Alexa-transferrin, an endocytic compartment marker, and (b) LysoTracker, which is specific for lysosomes. Bars: 10 μm. Yellow and white arrows in (a) indicate the MTOC area.

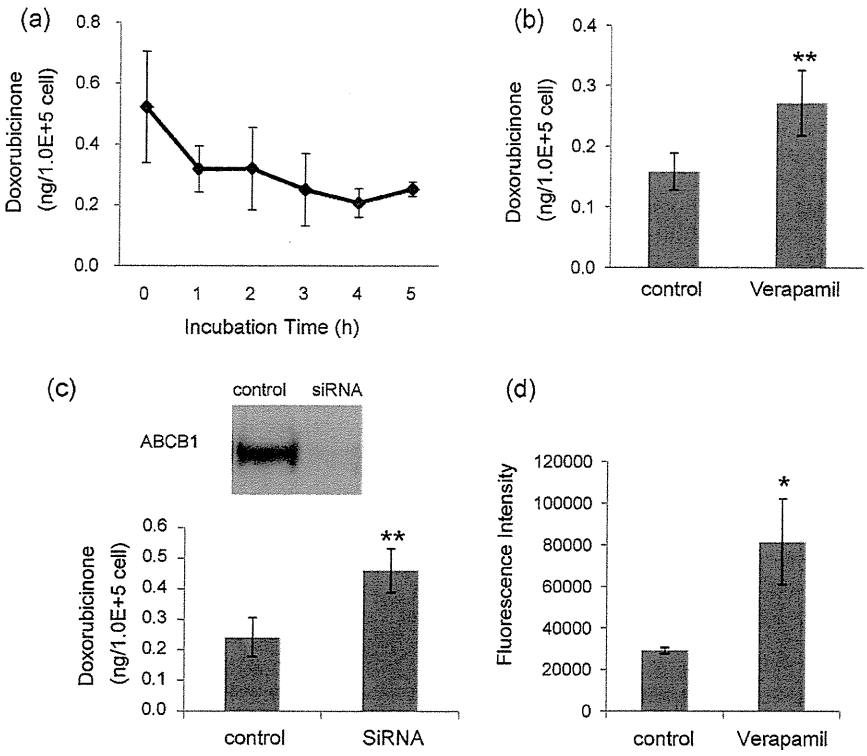

Fig. 7. Efflux of Dox-bound polymers. (a) Time-dependent change in intracellular Dox-bound polymers as indicated by released doxorubicinone. After incubation in medium with Dox-bound polymers, HeLa cells were washed and incubated with HBSS at 37 °C for the indicated durations. The doxorubicinone released by acid hydrolysis was quantitated as the amount of intracellular polymers as described in Section 2. (b) Effect of ABCB1 transporter on the efflux of Dox-bound polymers. HeLa cells were exposed to 50 μg/mL Dox-bound polymers in culture medium for 3 h. Cells were washed with 50 μg/mL verapamil or 0.1% dimethyl sulfoxide as a control. Then, the cells were incubated for another 2 h in HBSS containing the same concentration of each reagent. The amount of intracellular polymers was quantitated as the amount of doxorubicinone released by acid hydrolysis, as described in Section 2. $^{**}P < 0.01$. (c) Effect of the knockdown of ABCB1 transporter expression by siRNA on the efflux of Dox-bound polymers. Expression of ABCB1 in cell extracts was analyzed by immunoblot analysis (top). After 2 days of siRNA transfection, the cells were exposed to 50 μg/mL of Dox-bound polymers in culture medium for 3 h. After incubation, the cells were washed with HBSS and then incubated for another 2 h in HBSS without polymer. The amount of intracellular polymers was quantitated as the amount of doxorubicinone released by acid hydrolysis, as described in Section 2 (bottom). $^{**}P < 0.01$. Effect of ABCB1 transporter on the efflux of DBD-labeled polymers. HeLa cells were exposed to 50 μg/mL DBD-labeled polymers in culture medium for 24 h. Cells were washed with 50 μg/mL verapamil or 0.1% dimethyl sulfoxide as a control. Then, the cells were incubated for another 2 h in HBSS containing the same concentration of each reagent. The fluorescence intensity in a single cell was calculated as described in Section 2. $^{*}P < 0.05$.

in the ER might similarly gain access to the cytosol (Damm et al., 2005). The characteristic distribution pattern of the polymers did not change much with increasing incubation times from 0.5 to 24 h (data not shown). Although it is not clear whether the polymers maintain their structure as globular micelles or exist as unimers after internalization into a cell, increasing the dosed polymer concentration to 1 mg/mL did not change the staining pattern (data not shown). Recently, we showed PEG and poly(glutamic acid) block copolymer micelles incorporating dichloro(1,2-diaminocyclohexane)platinum(II) selectively dissociate within late endosomes (Murakami et al., 2011), suggesting that the Dox-bound polymers might also dissociate.

3.5. Efflux of Dox-bound polymers from HeLa cells to medium

As described in Section 3.2, the amount of intracellular Dox-bound polymers increased with time when cells were continuously exposed to Dox-bound polymers (Fig. 3a). In contrast, the amount of Dox-bound polymers gradually decreased after the Dox-bound polymers were removed from the medium (Fig. 7a). Interestingly, this decrease in the intracellular amount of Dox-bound polymers was abolished in the presence of verapamil, an inhibitor of ABCB1 (ATP-binding cassette protein B1) transporter (Fig. 7b). The ABCB1 transporter, which is also known as multidrug resistance 1 (MDR-1) or P-glycoprotein, is a member of the ABC-type transporter family and an efflux pump for various drugs. To further investigate the role of this transporter in the efflux of Dox-bound polymers from cells to medium, small interference RNAs (siRNAs) were used to target ABCB1 RNA in HeLa cells. Two days after transfection of synthetic siRNA, Western blot analysis showed that levels of ABCB1 protein expression in siRNA-transfected HeLa cells were drastically decreased (Fig. 7c), and the efflux of Dox-bound polymers from these cells was also significantly inhibited (Fig. 7c). The efflux of DBD-labeled polymers was also inhibited by ABCB1 transporter inhibitor, when intracellular fluorescent intensity of DBD-labeled polymers was measured (Fig. 7d). These results suggest that ABCB1 transporter is a key regulator of the clearance of Dox-bound polymers from HeLa cells.

It is reported that drug-binding site of ABCB1 transporter is located at a drug binding pocket that is formed by transmembrane segments and allow access of molecules directly from the membranes (Aller et al., 2009; Loo et al., 2003a,b). Furthermore, it is also known that subdomains of the ER form close contact with plasma membrane and some proteins may regulate the formation of direct membrane contacts that facilitate sterol exchange between the ER and plasma membrane (Ikonen, 2008).

Therefore, it is probable that a part of Dox-bound polymers localized in ER are transported to plasma membrane and then recognized at the drug binding site in the transmembrane segments of ABCB1 transporter.

In general, the ABCB1 transporter has very broad substrate specificity: recent studies have shown that it mediates the efflux

of a relatively large peptide, amyloid β peptide (molecular weight, 4.5 kDa), across the blood–brain barrier into the bloodstream (Cirrito et al., 2005; Kuhnke et al., 2007; Lam et al., 2001). To the best of our knowledge, the ABCB1 transporter has not been reported before to be involved in the clearance of block copolymers from cells. Because ABCB1 transporter is expressed primarily in certain normal cell types in the liver, kidney, and jejunum (Thiebaut et al., 1987), the role of ABCB1 transporter as excretion pump of Dox-bound polymer and the effect of ABCB1 transporter on the polymer blood level are probably significant from a safety perspective.

Taken together, the findings presented here suggest that Dox-bound polymers are incorporated by endocytosis. Some of the incorporated polymers are transferred to the endosome/lysosome system, and the rest may bypass the endosomal system. Then, the polymers are likely delivered to other compartments, including ER and the plasma membrane. The excretion of excess polymers from the cells is mediated by the ABCB1 transporter. Although in this system, the conjugated Dox was not designed to be released from the polymers, our results concerning intracellular trafficking and clearance of polymers would be very useful to design the carrier system where bound drugs are released from the carrier for pharmacological activity.

4. Conclusion

We investigated the intracellular trafficking of Dox-bound polymers. The polymers are internalized into cells by endocytosis, then transported to endosomal/lysosomal compartments, followed by partial distribution to the ER, or transported directly to the ER. The active excretion of the polymers from the cells may be mediated by the ABCB1 transporter. It is surprising that cells utilize their endogenous transport system for intracellular trafficking of this artificial drug carrier. Our results potentially can contribute not only to the discussion of safety issues of polymeric therapeutics but also the development of a DDS strategy utilizing or targeting this endogenous pathway more effectively.

Acknowledgements

The authors are grateful for support from Research on Publicly Essential Drugs and Medical Devices (Japan Health Sciences Foundation), a Health Labor Sciences Research Grant, and the Global COE Program for the Center for Medical System Innovation, MEXT, KAKENHI (21790046), and Nippon Kayaku Co. Ltd. We thank Mr. R. Nakamura (Nikon Corp.) for technical assistance.

References

Allen, C., Maysinger, D., Eisenberg, A., 1999. Nano-engineering block copolymer aggregates for drug delivery. Colloids Surf. B: Biointerfaces 16, 3–27.
Aller, S.G., Yu, J., Ward, A., Weng, Y., Chittaboina, S., Zhuo, R., Harrell, P.M., Trinh, Y.T., Zhang, Q., Urbatsch, I.L., Chang, G., 2009. Structure of P-glycoprotein reveals a molecular basis for poly-specific drug binding. Science 323, 1718–1722.
Bae, Y., Kataoka, K., 2009. Intelligent polymeric micelles from functional poly (ethylene glycol)-poly (amino acid) block copolymers. Adv. Drug Deliv. Rev. 61, 768–784.
Beyer, U., Rothern-Rutishauser, B., Unger, C., Wunderli-Allenspach, H., Kratz, F., 2001. Differences in the intracellular distribution of acid-sensitive doxorubicin-protein conjugates in comparison to free and liposomal formulated doxorubicin as shown by confocal microscopy. Pharm. Res. 18, 29–38.
Cirrito, J.R., Deane, R., Fagan, A.M., Spinner, M.L., Parsadanian, M., Finn, M.B., Jiang, H., Prior, J.L., Sagare, A., Bales, K.R., Paul, S.M., Zlokovic, B.V., Piwnica-Worms, D., Holtzman, D.M., 2005. P-glycoprotein deficiency at the blood-brain barrier increases amyloid-beta deposition in an Alzheimer disease mouse model. J Clin. Invest. 115, 3285–3290.
Damm, E.M., Pelkmans, L., Kartenbeck, J., Mezzacasa, A., Kurzchalia, T., Helenius, A., 2005. Clathrin- and caveolin-1-independent endocytosis: entry of simian virus 40 into cells devoid of caveolae. J. Cell Biol. 168, 477–488.
Davis, B.M., Humeau, L., Slepushkin, V., Binder, G., Korshalla, L., Ni, Y., Ogunjimi, E.O., Chang, L.F., Lu, X., Dropulic, B., 2004. ABC transporter inhibitors that are substrates enhance lentiviral vector transduction into primitive hematopoietic progenitor cells. Blood 104, 364–373.
Ferrari, M., 2005. Cancer nanotechnology: opportunities and challenges. Nat. Rev. Cancer 5, 161–171.
Hamaguchi, T., Kato, K., Yasui, H., Morizane, C., Ikeda, M., Ueno, H., Muro, K., Yamada, Y., Okusaka, T., Shirao, K., Shimada, Y., Nakahama, H., Matsumura, Y., 2007. A phase I and pharmacokinetic study of NK105, a paclitaxel-incorporating micellar nanoparticle formulation. Br. J. Cancer 97, 170–176.
Hopkins, A.L., Groom, C.R., 2002. The druggable genome. Nat. Rev. Drug Discov. 1, 727–730.
Hughes, B., 2009. Gearing up for follow-on biologics. Nat. Rev. Drug Discov. 8, 181.
Ikonen, E., 2008. Cellular cholesterol trafficking and compartmentalization. Nat. Rev. Mol. Cell Biol. 9, 125–138.
Illum, L., Davis, S.S., Müller, R.H., Mak, E., West, P., 1987. The organ distribution and circulation time of intravenously injected colloidal carriers sterically stabilized with a blockcopolymer-poloxamine 908. Life Sci. 40, 367–374.
Ioannou, Y.A., 2001. Multidrug permeases and subcellular cholesterol transport. Nat. Rev. Mol. Cell Biol. 2, 657–668.
Kataoka, K., Kwon, G.S., Yokoyama, M., Okano, T., Sakurai, Y., 1993. Block copolymer micelles as vehicles for drug delivery. J. Control. Rel. 24, 119–132.
Kataoka, K., Harada, A., Nagasaki, Y., 2001. Block copolymer micelles for drug delivery: design, characterization and biological significance. Adv. Drug Deliv. Rev. 47, 113–131.
Kolwankar, D., Glover, D.D., Ware, J.A., Tracy, T.S., 2005. Expression and function of ABCB1 and ABCG2 in human placental tissue. Drug Metab. Dispos. 33, 524–529.
Kuhnke, D., Jedlitschky, G., Grube, M., Krohn, M., Jucker, M., Mosyagin, I., Cascorbi, I., Walker, L.C., Kroemer, H.K., Warzok, R.W., Vogelgesang, S., 2007. MDR1-P-glycoprotein (ABCB1) mediates transport of Alzheimer's amyloid-β peptides – implications for the mechanisms of Aβ clearance at the blood–brain barrier. Brain Pathol. 17, 347–353.
Kuroda, J., Kuratsu, J., Yasunaga, M., Koga, Y., Saito, Y., Matsumura, Y., 2009. Potent antitumor effect of SN-38-incorporating polymeric micelle, NK012, against malignant glioma. Int. J. Cancer 124, 2505–2511.
Lam, F.C., Liu, R., Lu, P., Shapiro, A.B., Renoir, J.-M., Sharom, F.J., Reiner, P.B., 2001. β-Amyloid efflux mediated by p-glycoprotein. J. Neurochem. 76, 1121–1128.
Lavasanifar, A., Samuel, J., Kwon, G.S., 2002. Poly(ethylene oxide)-block-poly (L-amino acid) micelles for drug delivery. Adv. Drug Deliv. Rev. 54, 169–190.
Lee, S.M., Kim, J.S., 2005. Intracellular trafficking of transferrin-conjugated liposome/DNA complexes by confocal microscopy. Arch. Pharm. Res. 28, 93–99.
Lipinski, C.A., Lombardo, F., Dominy, B.W., Feeney, P.J., 2001. Experimental and computational approaches to estimate solubility and permeability in drug discovery and development settings. Adv. Drug Deliv. Rev. 46, 3–26.
Loo, T.W., Bartlett, M.C., Clarke, D.M., 2003a. Substrate-induced conformational changes in the transmembrane segments of human P-glycoprotein. J. Biol. Chem. 278, 13603–13606.
Loo, T.W., Bartlett, M.C., Clarke, D.M., 2003b. Methanethiosulfonate derivatives of rhodamine and verapamil activate human P-glycoprotein at different sites. J. Biol. Chem. 278, 50136–50141.
Manunta, M., Izzo, L., Duncan, R., Jones, A.T., 2007. Establishment of subcellular fractionation techniques to monitor the intracellular fate of polymer therapeutics. II. Identification of endosomal and lysosomal compartments in HepG2 cells combining single-step subcellular fractionation with fluorescent imaging. J. Drug Target. 15, 37–50.
Matsumura, Y., Maeda, H., 1986. A new concept for macromolecular therapeutics in cancer chemotherapy: mechanism of tumoritropic accumulation of proteins and the antitumor agent smancs. Cancer Res. 46, 6387–6392.
Matsumura, Y., Hamaguchi, T., Ura, T., Muro, K., Yamada, Y., Shimada, Y., Shirao, K., Okusaka, T., Ueno, H., Ikeda, M., Watanabe, N., 2004. Phase I clinical trial and pharmacokinetic evaluation of NK911, a micelle-encapsulated doxorubicin. Br. J. Cancer 91, 1775–1781.
Matteoni, R., Kreis, T.E., 1987. Translocation and clustering of endosomes and lysosomes depends on microtubules. J. Cell Biol. 105, 1253–1265.
Mineo, C., Anderson, R.G., 2001. Potocytosis. Robert Feulgen lecture. Histochem. Cell Biol. 116, 109–118.
Murakami, M., Cabral, H., Matsumoto, Y., Wu, S., Kano, M.R., Yamori, T., Nishiyama, N., Kataoka, K., 2011. Improving drug potency and efficacy by nanocarrier-mediated subcellular targeting. Sci. Transl. Med. 3, 64ra2.
Nakanishi, T., Fukushima, S., Okamoto, K., Suzuki, M., Matsumura, Y., Yokoyama, M., Okano, T., Sakurai, Y., Kataoka, K., 2001. Development of the polymer micelle carrier system for doxorubicin. J. Control. Rel. 74, 295–302.
Nishiyama, N., Kataoka, K., 2006. Current state, achievements, and future prospects of polymeric micelles as nanocarriers for drug and gene delivery. Pharmacol. Ther. 112, 630–648.
O'Brien, M.E.R., Wigler, N., Inbar, M., Rosso, R., Grischke, E., Santoro, A., Catane, R., Kieback, D.G., Tomczak, P., Ackland, S.P., Orlandi, F., Mellars, L., Alland, L., Tendler, C., 2004. Reduced cardiotoxicity and comparable efficacy in a phase III trial of pegylated liposomal doxorubicin HCl (CAELYX™/Doxil®) versus conventional doxorubicin for first-line treatment of metastatic breast cancer. Ann. Oncol. 15, 440–449.
Olson, R.D., Mushlin, P.S., Brenner, D.E., Fleischer, S., Cusack, B.J., Chang, B.K., Boucek Jr., R.J., 1988. Doxorubicin cardiotoxicity may be caused by its metabolite, doxorubicinol. Proc. Natl. Acad. Sci. U.S.A. 85, 3585–3589.

Rejman, J., Bragonzi, A., Conese, M., 2005. Role of clathrin- and caveolae-mediated endocytosis in gene transfer mediated by lipo- and polyplexes. Mol. Ther. 12, 468–474.

Richardson, S.C., Wallom, K.L., Ferguson, E.L., Deacon, S.P., Davies, M.W., Powell, A.J., Piper, R.C., Duncan, R., 2008. The use of fluorescence microscopy to define polymer localisation to the late endocytic compartments in cells that are targets for drug delivery. J. Control. Rel. 127, 1–11.

Sahay, G., Batrakova, E.V., Kabanov, A.V., 2008. Different internalization pathways of polymeric micelles and unimers and their effects on vesicular transport. Bioconjug. Chem. 19, 2023–2029.

Sahay, G., Alakhova, D.Y., Kabanov, A.V., 2010a. Endocytosis of nanomedicines. J. Control. Rel. 145, 182–195.

Sahay, G., Gautam, V., Luxenhofer, R., Kabanov, A.V., 2010b. The utilization of pathogen-like cellular trafficking by single chain block copolymer. Biomaterials 31, 1757–1764.

Sakai-Kato, K., Saito, E., Ishikura, K., Kawanishi, T., 2010. Analysis of intracellular doxorubicin and its metabolites by ultra-high-performance liquid chromatography. J. Chromatogr. B 878, 1466–1470.

Savić, R., Luo, L., Eisenberg, A., Maysinger, D., 2003. Micellar nanocontainers distribute to defined cytoplasmic organelles. Science 300, 615–618.

Thiebaut, F., Tsuruo, T., Hamada, H., Gottesman, M.M., Pastan, I., Willingham, M.C., 1987. Cellular localization of the multidrug-resistance gene product P-glycoprotein in normal human tissues. Proc. Natl. Acad. Sci. U.S.A. 84, 7735–7738.

Torchilin, V.P., 2002. PEG-based micelles as carriers of contrast agents for different imaging modalities. Adv. Drug Deliv. Rev. 54, 235–252.

Torchilin, V.P., Lukyanov, A.N., Gao, Z., Papahadjopoulos-Sternberg, B., 2003. Immunomicelles: targeted pharmaceutical carriers for poorly soluble drugs. Proc. Natl. Acad. Sci. U.S.A. 100, 6039–6044.

Yokoyama, M., Okano, T., Sakurai, Y., Fukushima, S., Okamoto, K., Kataoka, K., 1999. Selective delivery of adriamycin to a solid tumor using a polymeric micelle carrier system. J. Drug Target. 7, 171–186.

DDS製剤評価の動向と今後の課題

国立医薬品食品衛生研究所
薬品部 第4室 室長
厚生労働省 医薬食品局
審査管理課 併任
加藤 くみ子

1—はじめに

利便性、安全性、有効性を高めた高機能性製剤の開発が盛んに行われている。とりわけ、医薬品を“必要なときに、必要な場所で、必要な量だけ作用させる”ことを目的としたドラッグデリバリーシステム（DDS）技術の進展は、昨今のナノテクノロジー技術の発展と相まって高機能性製剤の開発原動力となっている。DDSの製剤開発の歴史は、1960年代の徐放性製剤の開発から始まり、現在までに経皮吸収型製剤、浸透圧ポンプ、リポソームなど多数の製剤が開発されている[1]。我が国においてもすでに1980年代より、リビッドマイクロスフェアのパルクス®、リプル®、またポリ乳酸・グリコール酸共重合体（PLGA）微粒子製剤のリューブリン®など優れたDDS製剤が開発・臨床応用されている。

投与経路の多様化に加え、DDSの技術にはデバイスを利用した技術、ポリマーやタンパク質などの高分子を利用した技術、あるいは製剤や原薬の物理的化学的な特性に工夫を凝らした技術など、1,400近くにも上るといわれている。本稿ではDDS製剤の主要技術となりつつあるナノテクノロジーを利用したDDS製剤（本稿ではナノDDS製剤と称する）を中心に、その評価の動向や今後の課題について考察したい。

2—ナノDDS製剤開発の動向

近年、ナノ医療（ナノメディシン）という言葉を耳にするが、ナノ医療で扱うスケールについては各地域の規制当局、さらに学術的な視点より異なると考えられる。

日本の規制当局においては現時点でナノメディシンの定義を定めていないが、本稿では、サブミクロン領域以下のナノメートルサイズの物質を含む「ナノDDS製剤」の意味で用いることとする。

我が国においては、1995年に公布・施行された科学技術基本法に基づき、科学技術の振興に関する施策の総合的かつ計画的な推進を図るため5年ごとに科学技術基本計画が策定されているが、2001年から開始された第2期科学技術基本計画の中で、ナノテクノロジーの医療への応用を推進することが示され、ナノメディシンに関わる研究が急速に促進されることとなった。

ナノDDS製剤としては、有効成分をキャリアであるリポソームや高分子ミセル等に内包させた内包型の製剤、有効成分に高分子あるいはタンパク質を結合させたコンジュゲート型の製剤が、我が国を含む世界中で市販あるいは開発されている。これらの多くは、有効成分を結合、または内包することで、生体内での放出性、標的性、生体内安定性等の体内動態を調節し、医薬品資源である有効成分の有用性を向上させた製剤である。また、ナノ結晶化製剤の登場に見られるように、ナノテクノロジーは、DDSの主要要素である吸収促進においてもその重要性を増している。

リポソーム製剤は国内外で10製品ほどが実用化されている。リポソームは内部に水相を有する脂質小胞であり、内水相や膜中に有効成分である薬物を保持できる。脂質膜組成の選択や表面修飾により，有効成分の体内動態を制御し，主薬理効果の向上、副作用軽減等の機能を付与することが可能である[2]。国内では、2004年以降3品目が承認されている（表）。腫瘍をターゲットとした多くのリポソーム製剤では病変部位における血管透過性の亢進を利用した（Enhanced permeation and retention effect：EPR効果[3]）、いわゆる受動的ターゲッティングが作用メカニズムの特徴となっている（図）。

ポリマー結合製剤は、有効成分である低分子化合物やタンパク質等にポリエチレングリコール（PEG）等のポリマーを結合した医薬品である。ポリマーを結合させることにより肝臓や脾臓などに存在する細網内皮系による貪食回避、安定性の向上、免疫原性低減、溶解性の向上等が期待される[4]。コンジュゲート型製剤としてスマンクス®が我が国において開発され1994年に発売されている他、PEGを結合したタンパク質、核酸医薬品が承

認されている。

一方、ナノ粒子製剤として、難溶性薬物のナノ結晶化製剤、酸化鉄微粒子等のMRI造影剤、人血清アルブミンと抗悪性腫瘍用薬であるパクリタキセルを結合したアブラキサン®等が代表例として挙げられる。ナノ結晶化製剤は薬物の結晶をナノメートルサイズに微小化することにより表面積を増加させ、溶出性や吸収性の向上を図った製剤である[5]。また、アブラキサン®は人血清アルブミンと有効成分であるパクリタキセルを結合させたナノ粒子製剤である。

3—ナノDDS製剤の評価について

1）国際的な規制の動き

ナノDDS製剤は生体高分子と同等なナノメートルサイズの構成要素を有するために、独特の生体内動態を示すとともに、電荷・表面積等の表面物性、形状等の物理的化学的要素を付加することにより、生体分子と様々な相互作用を有するように設計した製剤である。現状ではこれら医薬品の承認審査にあたっては、既存の規制システムの中で、個別の製品に応じた評価を行い承認されている。また既存のガイドラインを補完する形で新たな評価手法もケースバイケースで取り入れられている。しかしこのような製剤は従来の製剤とは体内での挙動や生体との相互作用など様々に異なるため、ナノDDS製剤の評価基準作成は国際的にも重要課題となっている。このような背景の中、欧州医薬品庁（European Medicines Agency：EMA）を中心とする国際的な専門家会議が開催されており、ナノDDS製剤に関する科学的見地からの 情報交換、情報収集を行っている。2010年9月2～3日には、EMAの主催による「ナノメディシンに関する第1回国際ワークショップ」が開催された[6]。この会議には欧州各国の他、米国、カナダ、日本、オーストラリアなど27カ国から開発企業、規制関係者、大学関係者、患者団体の代表等が出席し、①現在までにどのようなナノDDS製剤が実用化されてきたか、また開発中であるか、②医薬品への実用化に向け取り組まれている先進技術、③ナノDDS製剤の品質特性評価、非臨床評価、リスク管理（ヒト及び環境へのリスク評価）、④ナノDDS製剤を用いることによる患者の利益と利益享受のための課題、などが発表討議された。

2）米国におけるナノDDS製剤の規制動向

米国食品医薬品局(Food and Drug Administration：FDA)では約20品目のナノDDS製剤が承認されており、特にリポソーム製剤、ナノ粒子製剤が多く、それぞれ7品目、9品目（2010年9月現在）が承認されていることが、先に述べた第1回国際ワークショップで報告されている。

FDAより発出されている文書として、リポソーム製剤に関するガイドラインが2002年にドラフトとして出されている[7]。このガイドラインはCMC関連項目、ヒトでの薬物動態・生物学的利用能に関する項目、及び表示方法に関する項目から構成されている。

CMC関連項目では、製品の品質を左右する重要な品質特性パラメータの特定および測定、製品の一定性確保に必要な製造工程パラメータの特定およびその管理の重要性、有効成分およびキャリアである脂質の管理、製剤の安定性試験、製法変更時の留意事項が記されている。DDS製剤では、放出性、生体内安定性、標的性を付与するため添加物に様々な機能を付与する

表　日本で認可された主なナノDDS製剤[a]

分　類	商品名	薬効分類名	販売開始年
リポソーム製剤	ビスダイン®	加齢黄斑変性症治療剤	2004 年
	アムビゾーム®	ポリエンマクロライド系抗真菌性抗生物質製剤	2006 年
	ドキシル®	抗悪性腫瘍剤	2007 年
ポリマー結合製剤	スマンクス®	肝細胞癌治療剤	1994 年
	ペガシス®	ペグインターフェロンα-2a 製剤	2003 年
	ペグイントロン®	ペグインターフェロンα-2b 製剤	2004 年
	ソマバート®	成長ホルモン受容体拮抗剤	2007 年
	マクジェン®	加齢黄斑変性症治療剤	2008 年
ナノ粒子製剤	リゾビスト®	MRI 用肝臓造影剤	2002 年
	イメンド®	選択的 NK1 受容体拮抗型制吐剤	2009 年
	アブラキサン®	抗悪性腫瘍剤	2010 年

[a] 現時点で日本ではナノの定義が存在しないため、サブミクロン以下のナノメートルサイズの物質を含む医薬品を記した。

技術が重要となっている。FDAドラフトガイドラインでは、リポソーム製剤のキャリアに相当する脂質成分も添加物として記載されているが、その工程管理試験（材料＝脂質に関する厳重な管理）を重視していることが読み取れる。一方、ヒトでのPK試験とバイオアベイラビリティに関する項目では、①生体試料の分析法、②*in vivo*での完全性（integrity）の分析、③タンパク質の結合、④*in vitro*安全性、⑤PK試験とバイオアベイラビリティに関する留意事項が記載されている。*In vivo*での完全性（integrity）の分析、タンパク質の結合に関しては、薬効および有害作用（インフュージョン反応など）の作用メカニズムに関連した情報が品質管理の上でも重要であることを示すものであろう。

また、ドキソルビシン塩酸塩含有PEG修飾リポソーム製剤の後発品開発に関するドラフトガイダンスも2010年2月に出されている[8]。前提条件として、①後発医薬品と対照医薬品（先発医薬品）が同じ製剤組成を有していること、②硫酸アンモニウムグラジエントを用いたローディング法を利用して製造されていること、③物理的化学的特性が同等であること、が要求されており、そのうえで、生物学的同等性試験として、卵巣がん患者を対象とした臨床試験（遊離のドキソルビシンと内包されたドキソルビシンのAUCとCmax）、及び*in vitro*試験として粒子径分布、Dissolution testが記載されている。ナノDDS製剤のように高度に精密設計された製剤の同等性評価については、今後の重要課題である。

3）欧州におけるナノDDS製剤の規制動向

EMAでは、これまでに約18品目（2010年9月現在）のナノDDS製剤の販売承認申請の審査を行っていることが第1回国際ワークショップで報告されている。

薬効別では、抗悪性腫瘍用薬と免疫調節剤で約半数を占めており、また10製品がオーファンドラッグとして指定され、ナノDDS製剤が希少疾患の治療に大きく貢献していることが分かる。

EMAからのナノDDS製剤関連文書として、MRI造影剤等として利用されている酸化鉄ナノ粒子の後発品開発における非臨床試験に関するリフレクションペーパーが2010年に発出されている[9]。低分子化合物を有効成分とする後発医薬品では、有効成分が一旦循環血中に入るとその後の体内動態は標準製剤中の有効成分の動態と同じであると考えられる。従って、低分子化合物の水溶液である静脈注射用製剤の場合、原則として生物学的同等性は不要である。しかし、多くの注射用ナノDDS製剤に関しては、有効成分のキャリアもしくは有効成分そのものの物理的化学的特性を工夫し循環血中に入った後の有効成分の体内動態（標的部位や主要臓器への分布、代謝、排泄）を制御することを意図した製剤であるため、静脈注射用製剤であっても投与後の体内動態が重要であり、生物学的同等性が必要であると考えられる。さらに、ヒトにおける血中濃度とpKパラメータの比較に基づく生物学的同等性評価のみならず、標的部位や主要臓器への分布も安全性、有効性の観点から重要であるが、ヒトにおける試験は不可能であるため非臨床試験において標的部位や主要臓器への分布も含めた体内動態評価が重要であることの論理的根拠が記されている。具体的には、評価すべきコンパートメントとして血中、細網内皮系（脾臓、リンパ節、肝臓）、標的組織（薬理学的、毒性学的）を挙げ、これらのコンパートメントにおける鉄濃度測定の重要性を指摘している。本リフレクションペーパーで示されている指針は、今後のナノDDS製剤開発に当たり非常に有用な示唆を与えると考えられる。

4）我が国におけるナノDDS製剤評価

我が国においては、現時点でナノDDS製剤評価の規制に関連した文書は出されていない。しかし、新規素材をキャリアとし抗癌剤等の標的部位への送達、放出制御を狙った製剤は世界に先駆けて進行中である。従って、ファースト・イン・ヒューマン試験までに必要な評価項目も含め、ナノDDS製剤の開発、承認申請において配慮すべきポイントを明確にし、さらには評価ガイドライン等としてまとめることが危急の課題

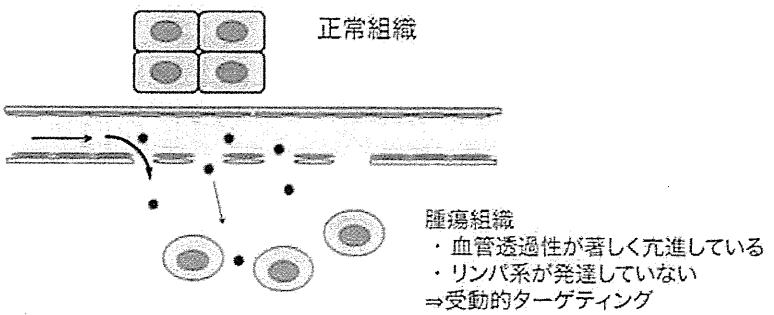

図　EPR効果の模式図[3]

となっている。現在、産官学連携の枠組みの中で、ナノDDS製剤の評価に関する研究・議論を行っており、以下に一部紹介したい。

我々は、ナノDDS製剤のサイズ評価、表面物性評価など物理的化学的評価手法に関する研究を行っている。医薬品の品質管理を合理的に行う上で、品質、有効性、安全性を左右する重要品質特性を特定し、有効性、安全性に悪影響を与えない重要品質特性パラメータの許容範囲を捉えることが重要である。例えば多くのナノDDS製剤においては、病変部位への標的性、バイオアベイラビリティの向上など、ナノメートルという微小な大きさによる“サイズ効果”が重要な要素であることから、サイズ（粒子であれば粒子径）及びサイズ分布幅が重要品質特性の一つと言えるであろう。その他、ゼータ電位等の表面物性、機能性を付与するための表面修飾に関する物理的化学的特性についても製品ごとの特性に応じて評価されうるべきであろう。これらの特性を評価しうる分析手法の整備は、今後の科学的課題である。さらに、これまで述べてきたようにナノDDS製剤の体内動態（全身レベルから組織・器官レベル、さらに製品によっては細胞レベル、細胞小器官レベルに至るまで）に関するデータ、さらには情報が必要である。その上で、ナノDDS製剤の体内動態と品質特性の関係に関する知識を蓄積し、体内動態に重要な影響を及ぼす製剤の重要品質特性を明らかにする。同様に、体内動態と医薬品としての有効性・安全性との関係に関する知識、重要品質特性に影響する製造工程パラメータに関する知識を蓄積することにより、ナノDDS製剤の的確な製剤設計、合理的な製法・品質管理システムが構築されると考えている。

5）ナノDDS製剤の情報収集について

米国、カナダにおいては審査段階にあるナノマテリアルを含む医薬品に関する情報収集、データベース化の整備が進められている。データベース化された情報は非公開である。既にFDAでは、審査段階にあるナノマテリアルを含む医薬品に関する情報収集、データベース化が一部開始されている[10]。また、カナダ厚生省においては暫定的にナノマテリアルに対する作業定義を定め、医薬品の治験申請及び新薬申請時にナノマテリアルの含有に関する記載を求めている[11]。このようなナノDDS製剤に関する情報収集手段の構築は、現在のサイエンスでは予想不可能な事態が臨床上で生じた際に迅速な対応を図る上で非常に重要であると思われる。また、得られた情報は審査における知識の蓄積や市販後の安全性（申請資料から得られる情報からでは分からないこと、たとえば、長期服用による影響など）に関する情報収集等を円滑に行う上でも有用であろう。また、ナノDDS製剤に関連した政策決定に利用できる、という利点も挙げられるだろう。

4—おわりに

治療と診断を融合した複合技術であるセラノスティック（Theranostic：TherapyとDiagnosticを融合した造語）など、新たに現われつつある融合技術も含め、DDS製剤の品質、安全性、有効性を適切に評価するための十分な科学的基礎を築くために、産官学連携の枠組みにおける継続的な対話と、更なる科学的研究が重要であると思われる。

参考文献

1) ポストゲノムの医薬品開発とDDS技術の新展開　HS振興財団：HSレポートNo.63, 2008
2) 菊池寛, Pharm Tech Japan 25: 2700-2703, 2009
3) Matsumura Y, Maeda H, Cancer Res 46: 6387-6392, 1986
4) Duncan R, Nature Rev Cancer 6: 688-701, 2006
5) 森部久仁一, ファルマシア45: 1217-1221, 2009
6) 1st International Workshop on Nanomedicines 2010 Summary Report, European Medicines Agency 2010
7) Liposome Drug Products－Chemistry, Manufacturing, and Controls; Human Pharmacokinetics and Bioavailability; and Labeling Documentation, US Food and Drug Administration, 2002
8) Draft Guidance on Doxorubicin Hydrochloride, US Food and Drug Administration, 2010
9) Reflection paper on non-clinical studies for generic nanoparticle iron medicinal product applications, European Medicines Agency, 2010
10) MANUAL OF POLICIES AND PROCEDURES (MaPP) 5015.9 Reporting Format for Nanotechnology-Related Information in CMC Review, US Food and Drug Administration, 2010
11) Drug Submission Application Form for: Human, Veterinary or Disinfectant Drugs and Clinical Trial Application/Attestation, Health Canada

加藤 くみ子　かとう・くみこ
国立医薬品食品衛生研究所 薬品部 第4室 室長
厚生労働省 医薬食品局 審査管理課 併任
山梨県生まれ
東京大学 薬学部卒
東京大学大学院 薬学系研究科 修士課程修了
薬学博士
専門は薬剤学、分析科学

Genome-wide association study of SSRI/SNRI-induced sexual dysfunction in a Japanese cohort with major depression

Kouichi Kurose[a,*], Kazuyuki Hiratsuka[b], Kazuya Ishiwata[a, b], Jun Nishikawa[a], Shinpei Nonen[c], Junichi Azuma[c, d], Masaki Kato[e], Masataka Wakeno[e], Gaku Okugawa[e], Toshihiko Kinoshita[e], Toru Kurosawa[b], Ryuichi Hasegawa[a], and Yoshiro Saito[a]

[a]Division of Medicinal Safety Science, National Institute of Health Sciences, Tokyo, Japan

[b]Pharmaceutical Research Center, Meiji Seika Pharma Co., Ltd. Kanagawa, Japan.

[c]School of Pharmacy, Hyogo University of Health Science, Hyogo, Japan

[d]Graduate School of Pharmaceutical Sciences , Osaka University, Osaka, Japan

[e]Department of Neuropsychiatry, Kansai Medical University, Osaka, Japan

[*]Corresponding author: Division of Medicinal Safety Science, National Institute of Health Sciences, 1-18-1 Kamiyoga, Setagaya-ku, Tokyo 158-8501, Japan

Tel.: +81-3-3700-1141, FAX: +81-3-3700-9788, E-mail: kurose@nihs.go.jp

Abstract

Sexual dysfunction is a major side effect of selective serotonin reuptake inhibitors (SSRIs) and serotonin–noradrenaline reuptake inhibitors (SNRIs). We conducted a genome-wide association study to identify the genetic factors contributing to the risk of SSRI/SNRI-induced sexual dysfunction by testing 186,320 SNP markers in a cohort of 201 Japanese major depression patients including 36 with sexual dysfunction induced by SSRI (paroxetine or fluvoxamine) or SNRI (milnacipran). The Cochran–Armitage trend test showed that 11 SNPs, tightly clustered in a distinct region on chromosome 14q21.3, were associated with SSRI/SNRI-induced sexual dysfunction at a genome-wide significance level after FDR correction, and the strongest SNP association was with rs1160351 ($P = 3.04 \times 10^{-7}$, risk ratio = 2.92, 95% CI = 1.79–4.76). These SNPs mapped to the intronic region of the *MDGA2* gene.

A Manhattan plot showed that the strong association peak remained in *MDGA2* after adjustment for sex and age in a multivariable logistic regression analysis although *P* values increased slightly and became nonsignificant. Replication studies with larger sample sizes are required to validate this exploratory study, but our findings may provide insights into the genetic basis of sexual dysfunction induced by SSRI/SNRI.

Key words: pharmacogenomics; pharmacogenetics; GWAS; adverse drug reaction; antidepressant; norepinephrine.

1. Introduction

Genetic factors contribute to individual variations in drug efficacy and adverse reactions to selective serotonin reuptake inhibitors (SSRIs) and serotonin–noradrenaline reuptake inhibitors (SNRIs) (Malhotra et al., 2004; Serretti and Artioli, 2004; Kato et al., 2006; Serretti et al., 2007; Kato et al., 2008; Wakeno et al., 2008; Ising et al., 2009; Kato et al., 2009; Thomas and Ellingrod, 2009; Kato and Serretti, 2010). Sexual dysfunction caused by SSRIs and SNRIs is a common adverse side effect that can have a significantly adverse impact on a patient's quality of life and can lead to noncompliance with medication. To our knowledge, only two pharmacogenomic studies concerning SSRI-induced sexual dysfunction have been reported until date. These studies involved candidate gene approaches that suggested that polymorphisms of the serotonin 2A receptor gene (*HTR2A*) and glutamate receptor genes (*GRIA3*, *GRIK2*, *GRIA1*, and *GRIN3A*) are associated with SSRI-induced sexual dysfunction (Bishop et al., 2006; Perlis et al., 2009). However, diverse physiological pathways are potentially involved in sexual dysfunction pathology; thus, unpredictable genetic factors may be involved in the pathogenesis of this adverse reaction. In this study, we conducted a genome-wide association study (GWAS), rather than a candidate gene approach, to identify the genes or genetic biomarkers associated with SSRI/SNRI-induced sexual dysfunction. GWAS approaches can survey the entire genome using a hypothesis-free approach to detect the genetic variations associated with the phenotype of interest. GWAS has actually identified genetic risk factors associated with drug-induced adverse reactions (Link et al., 2008; Daly et al., 2009; Ozeki et al., 2011). The present study describes the first pharmacogenomic GWAS of sexual dysfunction induced by antidepressants. This study has some potential limitations such as a relatively small sample size and lack of a replication study with other independent samples. However, our exploratory study represents an important first step in applying GWAS to identify the genetic causes of SSRI/SNRI-induced sexual dysfunction.